Surface and bulk band-structure effects on $CoSi_2/Si(111)$ ballistic-electron emission experiments

K. Reuter* and P. L. de Andres
Instituto de Ciencia de Materiales (CSIC), Cantoblanco, E-28049 Madrid, Spain

F. J. Garcia-Vidal and F. Flores
Departamento de Física Teórica de la Materia Condensada (UAM), E-28049 Madrid, Spain

K. Heinz
Lehrstuhl für Festkörperphysik, Universität Erlangen-Nürnberg, Staudtstraße 7, 91058 Erlangen, Germany
(Received 19 December 2000; published 7 May 2001)

A theoretical model of ballistic-electron-emission microscopy (BEEM) based on linear combination of atomic orbitals Hamiltonians and Keldysh Green's functions is applied to analyze experimental data obtained for $CoSi_2/Si(111)$ contacts. Hot electrons injected from a scanning tunneling microscope tip into the silicide film form a highly focused beam, which even after propagation through films of moderate thickness is narrow enough to allow the observed atomic resolution of interfacial point defects. On (2×1) reconstructed domains a certain fraction of the initial current is injected into localized surface states, leading to the reported contrast in BEEM images, reflecting the topography at the surface. These results confirm that band-structure effects, both in the bulk and at the surface of the metallic overlayer, intricately influence the interface-related information contained in BEEM data. It is found that for a careful analysis of experimental results, a theoretical model going beyond the ballistic hypotesis is required.

DOI: 10.1103/PhysRevB.63.205325 PACS number(s): 73.20.At, 72.10.Bg

I. INTRODUCTION

In ballistic-electron-emission-microscopy (BEEM) electrons are injected locally by a scanning tunneling microscope (STM) tip into a metallic film grown on a substrate semiconductor.[1] This is a remarkable experimental set up that has extended the power of the STM to investigate surfaces to an object well buried underneath the metal-semiconductor interface. The standard model distinguishes four relevant steps for the process: (i) tunneling, (ii) transport in the metallic film, (iii) transmission through the Schottky barrier, and (iv) transport through the semiconductor.[2] As the outcome of any of these steps is linked to physical processes affecting other steps, a theoretical model setup to derive physical conclusions from experimental data has to treat all the steps with enough care to avoid cross-correlations between physical effects leading to spurious conclusions.[3] In particular, the initial theoretical models set up to interpret the measured *I-V* characteristic have assumed WKB planar theory and ballistic propagation of electrons, making it difficult to explain a number of experimental findings, most notably the nanometric lateral resolution after propagation by metal films more than 100-Å thick.[4] Therefore, theoretical efforts to improve the model have included semiclassical *E* space[5,6] or *k* space[7] Monte Carlo simulation, *ab initio* calculation of the transmission through the metal-semiconductor interface,[8] and a Keldysh Green's functions formalism.[9]

From an experimental point of view, BEEM experiments on silicides-silicon interfaces can be made with remarkable precision due to the small mismatch between lattices in the interface.[10] Furthermore, vacuum and low-temperatures techniques can greatly facilitate the theoretical interpretation of experimental data. In this paper we shall be mainly concerned with two different kinds of experimental results that within the framework of our theory appear to be related to electronic structure effects. First, atomic or nearly-atomic resolution is observed in the BEEM image formed at the interface. This has been demonstrated by imaging a point defect,[11] that usually is taken as the definitive test for the resolution in the STM technique. Second, in the same image a curious anticorrelation between the STM and the BEEM images is found. Working under usual conditions (i.e., constant tunneling current injected into the metal), the BEEM image taken under a 2×1 reconstructed patch on the surface shows the same periodicity, but maxima and minima have been interchanged between both techniques.

II. THEORETICAL

A. Formalism

For the inclusion of band-structure effects into a theoretical model of BEEM we set up a linear combination of atomic orbitals (LCAO) scheme, computing fully quantum mechanically the elastic component of the BEEM current inside the metal film. In this localized basis, the total Hamiltonian may then be separated into three terms

$$\hat{H}=\hat{H}_T+\hat{H}_S+\hat{H}_I, \tag{1}$$

where $\hat{H}_T=\Sigma\epsilon_\alpha\hat{n}_\alpha+\Sigma\hat{T}_{\alpha\beta}\hat{c}_\alpha^\dagger\hat{c}_\beta$ defines the tip, $\hat{H}_S=\Sigma\epsilon_i\hat{n}_i+\Sigma\hat{T}_{ij}\hat{c}_i^\dagger\hat{c}_j$ describes the metal sample, and $\hat{H}_I=\Sigma\hat{T}_{\alpha m}\hat{c}_\alpha^\dagger\hat{c}_m$ represents the coupling between the tip and the surface in terms of a hopping matrix, $\hat{T}_{\alpha m}$ ($\hat{n}_\alpha$, $\hat{c}_\alpha^\dagger$, and $\hat{c}_\alpha$ are number, creation, and destruction operator defined in the usual way). Note, that we use greek indices for tip sites and

latin indices for sites inside the metal sample. Useful tight-binding parameters can be introduced by fitting *ab initio* calculations for the metal sample. Whereas T_{ij} is obtained from the same fitting procedure, we approximate the hopping matrix between tip and sample, $\hat{T}_{\alpha m}$, by allowing only tunneling between the *s* orbitals of one active site $\alpha=0$ in the tip and sites *m* in the sample. This approximation, known to be poor for the general STM problem at small tip-sample distances, is justified in the BEEM context, where tip-surface distances are large, typically more than 6 or 7 Å .

We are interested to calculate currents in the coupled tip-sample system, which is a nonequilibrium problem because the existence of a finite bias. Based on earlier work by Caroli *et al.*[12] we have shown previously in detail,[3,13] that with the help of the Keldysh Green's function technique the current between two sites *i* and *j* in the metal after injection from a single tip site (0) can be obtained from the following formula:

$$J_{ij}(E,r_{\|})=\frac{4e}{\hbar}\mathrm{Im}\,\mathrm{Tr}\sum_{mn}\,[\hat{T}_{0n}\hat{g}^{A}_{ni}(E,r_{\|})\hat{T}_{ij}\hat{g}^{R}_{jm}(E,r_{\|})\hat{T}_{m0}\hat{\rho}_{00}]. \tag{2}$$

Here, the internal summation runs over all tunnel-active sites, *m* and *n*, in the sample surface. $\hat{\rho}_{00}$ is the density of states matrix of the tip, and the trace denotes summation over the atomic orbitals forming the LCAO basis. Finally, $\hat{g}^{R}_{jm}$ and $\hat{g}^{A}_{ni}$ are the retarded and advanced equilibrium Green's functions of the metal respectively, describing the propagation of electrons and holes between the corresponding sites given in the indices. We notice that this formula only involves solutions for the tip and sample Hamiltonians before any interaction is switched on, and the knowledge of the hopping matrices coupling tip and sample. The power of the Keldysh technique employed to arrive at this formula is hence that the latter applies properly for a nonequilibrium situation under any given bias, involving only equilibrium quantities that belong to the separated subsystems, which are easily calculated.

In fact, the main quantities left to calculate are the retarded Green's functions for a metallic surface. These are easily obtained in an iterative way, where one starts with a small slab and progressively doubles the size of the latter, until both of its surfaces are effectively decoupled, so that the end product are the propagators of a quasi-semi-infinite metal film. The underlying decimation technique[14,15] takes advantage of the fact, that not all matrix elements of the Green's function matrix are required, but only the ones connecting atomic sites *m* and *n* in a surface layer with the sites *i* and *j* inside the film. Hence, a set of coupled linear equations is set up, which only input in every new iteration is the output of the preceding one, keeping the total number of involved matrix elements constant. As we have described this procedure in detail before,[16,17] suffice it here to mention that in the construction of the initial Green's functions a small, but finite imaginary part $i\eta$ is added to the energy *E* to ensure mathematical convergence. This η can also be used to introduce an attenuation to the wave field, thus mimicking inelastic effects. In this work, a value of $\eta=0.05$eV was chosen to reproduce the experimentally measured attenuation length.[18]

As the same bulklike layers are iteratively doubled in the decimation technique, the $\hat{g}^{R,A}_{jm}$ created are necessarily the propagators inside a metal film with an ideal-terminated surface (i.e., without reconstructions or relaxations). While this is usually quite a good approximation, it might be not so appropriated for the ultrathin-$CoSi_2$ films, or for some reconstructed patches of the surface we need to consider. Therefore, as a final step we use the Dyson equation and a local neutrality charge condition to couple a surface superlayer with differing geometric and electronic structure to the bulk-terminated semi-infinite slab.[17] For this surface layer an additional set of parameters is required, whose determination will be addressed in the following section.

When $J_{ij}(E)$ is computed for all atoms *i* inside a given layer in the metal, with current contributions from all respective neighbors *j* in layers above, a two-dimensional (2D) current distribution in real space is obtained. If this procedure is repeated for several layers parallel to the surface at different depths, the shape of the electronic beam propagating through the metal can be retrieved. Although the calculations are done within a semi-infinite metal slab, the current distribution at any layer *i* will give a good approximation of the current impinging on a semiconductor interface after propagation through a finite metal film with a thickness corresponding to the chosen layer *i*. With this, the experimentally observed high spatial resolution can already be addressed.

However, in order to really calculate the actual BEEM current, the current distribution arriving at the interface needs to be matched with available states in the semiconductor. We will discuss below that at an almost perfect epitaxial interface, like the $CoSi_2/Si(111)$ one, one might expect that $\mathbf{k}_{\|}$ is conserved for a dominant fraction of the current. Therefore, we additionally need to calculate not only real-space current distributions, but also the momentum distribution, between any two layers *i* and *j* as a function of $\mathbf{k}_{\|}$. For this one can derive an analogous expression to Eq. (2),[3,13]

$$J_{ij}(E,k_{\|})=\frac{4e}{\hbar}\mathrm{Im}\,\mathrm{Tr}\sum_{mn}\,[\hat{T}_{0n}\hat{g}^{A}_{ni}(E,k_{\|})\hat{T}_{ij}\hat{g}^{R}_{jm}(E,k_{\|})\hat{T}_{m0}\hat{\rho}_{00}] \tag{3}$$

where all quantities are the $\mathbf{k}_{\|}$-Fourier transforms of the corresponding objects in Eq. (2). This current can be thought as the joint probability for an electron to hop from the tip (0) to a layer in the surface (m), $\hat{T}_{m0}\hat{\rho}_{00}$, to be propagated to layer (j) by the retarded Green's function $\hat{g}^{R}_{jm}$ and finally to hop to layer (i), $\hat{T}_{ij}$, while a hole is propagated by the advanced Green's function $\hat{g}^{A}_{ni}$ between layers (i) and (n), hopping back to the tip, $\hat{T}_{0n}$. To get a quantitative result for a specified-tip voltage *V*, this momentum distribution has to be matched with the available conduction-band minima in the semiconductor, resulting in a quantum mechanical transmission factor, $T(E,\mathbf{k}_{\|})$ (that might be modified to take into account other effects due to the backscattering of electrons from the semiconductor). Finally, to compute the *I-V* char-

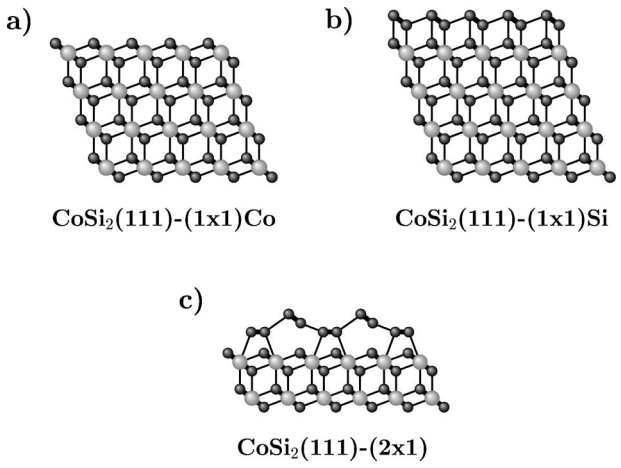

FIG. 1. Cross-sectional projection onto the $(1\bar{1}0)$ plane of the (a) $CoSi_2(111)$-(1×1) Co-rich, (b) $CoSi_2(111)$-(1×1) Si-rich, and (c) $CoSi_2(111)$-(2×1) surface structure. Bonds parallel to the projection plane are drawn as thin lines. Bonds that point out of the projection plane (i.e. by 60°) are plotted as thick lines. Co atoms are indicated with light bigger spheres and Si atoms with dark-smaller spheres.

acteristics one must integrate up for all energies from the Schottky barrier to eV and all allowed $\mathbf{k}_\parallel$ in the interface Brillouin zone

$$I(V)=\int_{eV_0}^{eV} dE \int_{IBZ} dk_\parallel J(E,k_\parallel)T(E,k_\parallel). \tag{4}$$

While this procedure has been successfully applied to deduce electron-electron attenuation lengths from fits to experimental Au/Si(111) BEES $I(V)$ spectra,[19,20] we shall argue below, that in the present case a simpler approach just integrating up the total current at any layer i is sufficient to explain the anticorrugation contrast for the $CoSi_2(111)$-(2×1) surface phase.

B. $CoSi_2$ material parameters

In addition to the general setup of our theoretical approach, the ultrathin films employed in the $CoSi_2$/Si BEEM experiments require a careful implementation not only of bulk, but also of surface-related material parameters. Effects like the anticorrugation contrast must have their origin in an intricate interplay of geometric and electronic structure at the film boundary, entailing the necessity of an accurate modeling of both system properties. Within our non-self-consistent approach, we have to rely on empirical parameters for this task, which we obtain from existing experimental or theoretical data. The accuracy of this procedure is finally cross checked by comparing with available *ab initio* calculations.

1. Geometric surface structure

$CoSi_2$ crystallizes in the well-known CaF_2 structure.[21] Seen along the $\langle111\rangle$ direction, a Si_1-Co-Si_2 trilayer stacking sequence of hexagonal Bravais planes results, as shown in Fig. 1. Two different (1×1) surface phases can be found, depending on the particular growth conditions:[22,23] Annealing at lower temperatures after RT codeposition stabilizes the so-called Co-rich termination, while higher temperatures ($>550\,^\circ$C) lead to Si segregation and to the formation of the alternative Si-rich termination, as shown in Fig. 1(a) and 1(b) respectively. Stalder *et al.*[24] reported an additional (2×1) reconstruction, coexisting with the Si-rich phase on ultrathin ($d<45$ Å), epitaxial $CoSi_2$ films on Si(111). As the experimental preparation of pin-hole free samples involves a final annealing step,[10] only the Si-rich (1×1) and (2×1) phases are encountered in the BEEM context.

A recent quantitative low-energy electron diffraction (LEED) study[25] revealed the topmost crystallographic arrangement of the (1×1) Si-rich phase as a Si bilayer on top of the last Si_1-Co-Si_2 trilayer of the bulk stacking sequence, thus achieving an ideal bulklike fourfold and eightfold coordination for the Si_1 and Co atom, respectively, cf. Fig. 1(b). The Si-Si bilayer itself exhibits a considerably larger thickness (0.91 Å) than the corresponding 0.78 Å in bulk Si. The distance to the trilayer below is expanded by $\approx6\%$ in comparison to the trilayer-trilayer spacing deep inside $CoSi_2$. As the last noticeable change of this multilayer-relaxation sequence, the following Si_1-Co spacing within the first trilayer underneath is also compressed ($\approx9\%$). These exact parameters have been used as geometric input structure for the Si-rich (1×1) phase, whereas a slight-lateral expansion of the complete $CoSi_2$ film (0.5%) as suggested by the LEED results has been neglected.

Unfortunately, no such detailed crystallographic data is presently available for the (2×1) reconstruction. As a guideline, STM images clearly show (2×1) chains perpendicular to the three $\langle2\bar{1}\bar{1}\rangle$ directions.[24] In analogy to Pandey's π-bonded chain model for the Si(111)-(2×1) surface, the structure displayed in Fig. 1(c) was hence proposed.[24] Since this reconstruction is only seen under conditions where usually the Si-rich (1×1) phase is stable, the (2×1) chains should derive from a backbond flip of the top trilayer Co atom to the additional Si bilayer. While in the (1×1) situation, cf. Fig. 1(b), the lower Si bilayer atom is bound to the Co atom located directly below, this bond flips now to a neighboring top atom in the Si bilayer. As a natural consequence, the top atom is depressed and attracted along $\langle2\bar{1}\bar{1}\rangle$ towards the new bonding Co atom, leading to the formation of the low chains. On the other hand, the Si atom, which has lost its backbond, rises and saturates via π bonds within the Si bilayer. Focusing on point defects in this high chain, the STM images suggest a tilting of the two elevated-Si atoms, such that the orientation of the high chain is the same as the one of the bulk trilayers as depicted in Fig. 1(c). Lacking a precise structural analysis, a symmetrized and simplified version of this model was employed for the BEEM computations: the top Si_1-Co-Si_2 trilayer has been left with bulk spacings, while the position of all Si chain atoms is determined by trying to keep the Si-Si bond lengths at the ideal 2.35 Å bulk value wherever possible. The details of this model and its implications on the electronic surface structure have been described elsewhere,[26] where we also reported on the agreement we achieve with existing experimental data.

For the tunneling between the tip and these surface structures we apply a WKB derived exponential damping, valid because the tip-sample distance in BEEM is rather large. The triangular shaped potential barrier used in this formalism is determined from the known work functions of the tungsten tip and the metal, $\Phi_T(\mathrm{W}) = 4.80$ eV and $\Phi_S(\mathrm{CoSi_2}) = 4.70$ eV, respectively.[2,27] We allow hopping to all lattice sites, m and n [cf. Eq. (2)], within a given radius r_T around the tip apex positioned at 5-Å height. This radius was progressively increased until no further changes occurred in the obtained results. For the real-space images convergence was rapidly reached at $r_T = 7$ Å , involving on average some eight atoms in the topmost layer in the injection event, depending on the chosen lateral tip position. A larger value of $r_T = 10$ Å was required for the more delicate calculations in reciprocal space, entailing this time about 30 active tunneling sites.

2. Electronic surface structure

As described above, our theoretical approach is based on a LCAO Hamiltonian within the two-center approximation introduced by Slater and Koster.[28] The required tight-binding (TB) parameters for bulk $CoSi_2$ have been determined by Sanguinetti *et al.*, including next-neighbor interaction within each and in between all three sublattices of the CaF_2-type lattice.[29] The extended basis of sp^3 for Si and sp^3d^5 orbitals for Co with the inclusion of *d-d* hopping elements between the metal atoms reproduces accurately the overall bulk band structure as obtained from *ab initio* calculations.[30,31] Notwithstanding, the focus in BEEM is particularly on the small region from the Fermi level until some few eV above. We have found that a slight modification of the parameters of Sanguinetti *et al.* in form of rigidly shifting the on-site energies by 0.3 eV manages to model most reliably especially those bands that will be relevant in the later application without much affecting the quality of the fit in the remaining energy range. Note, that only with this shift, the delayed BEEM onset discussed below and already found in the prior *ab initio* calculations[31] is properly obtained. Independent of the shift, the TB approximation becomes less accurate for the high-energy conduction bands above $E \approx 2.0$ eV, so that we will focus on BEEM energies above the threshold dictated by the Schottky barrier, but below this upper limit.

The Slater-Koster parameters, which are obtained through fits to the bulk band structure, can obviously not take into acount effects due to the truncation of bonds at the surface. In principle, another self-consistent calculation determining the new charge distribution would be required, to which a new set of surface TB parameters could be adjusted. However, already quite accurate results can be obtained with the help of a balancing Coulomb potential, which imposes a layerwise local charge neutrality by modifying the diagonal part of the Hamiltonian matrix.[15] The fitted values of this artificial dipole potential for all described $CoSi_2$ surface phases can be found in Ref. 26, where the resulting electronic structure of the (2×1) reconstruction is discussed in detail. While we already achieved very good agreement with existing experimental data in the latter case, we further checked the accuracy of our proceeding with the Co-rich (1×1) phase, that is not relevant in the BEEM context, but which is the only phase for which an *ab initio* investigation has been performed.[32] Again we find very good agreement, reproducing well all surface related features present in form of three resonances that had also been described experimentally.[33] These findings confirm that an appropriate picture of the surface electronic structure can be retrieved within our approach, which does not aim at a precise modeling of the latter quantity itself, but uses its predominant features to discuss the effects on BEEM data.

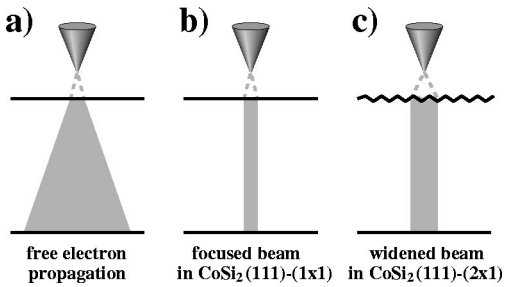

FIG. 2. Schematic picture of the shape of the electron beam propagating through the metal film. (a) Conical shape according to the free-electron model of BEEM, (b) focused beam of constant width due to the $CoSi_2$ band structure, and (c) increased beam diameter under a (2×1)-reconstructed surface.

III. RESULTS

A. Nanometric interface resolution

The nanometric resolution, with which individual point defects have been detected, reflects the spatial extent of the electron beam scanning the interface, rather than the real size of the probed object itself. In the simple free-electron model of BEEM, this beam has a conical shape, with a pointlike injection at the surface and a typical polar opening angle of $\approx 40°$ due to the uncertainty in parallel momentum, cf. Fig. 2(a).[2] Already for the ultrathin- 28-Å films used in the earlier experimental study by Meyer and von Känel,[34] a beam diameter of about 25 Å would result, which is by a factor of 2 off the experimental resolution with a full width at half maximum (FWHM) of (11 ± 2) Å . In order to analyze this problem with our formalism, we calculate real and reciprocal space current distributions in a layer parallel to the surface and located at a depth equivalent to this experimental film width.

1. A quasiatomically focused beam

Experimentally, the high-resolution capability has been asserted over quite a range of tip voltages, rising above the noise level at about $E \approx 0.8$ eV, reaching its maximum at $E \sim 1.5$ eV, before decreasing gradually above $E \sim 2.0$ eV.[34,35] This degradation at higher biases is not necessarily related to the elastic electron propagation itself, but most probably due to a progressively increased share of secondary carriers. In the next subsection we will show that the high resolution is due to the particular form of an electron band, which leads to a virtually unchanged transport pattern within the energy range 0.9 eV $< E <$ 2.5 eV. While we verified this by test calculations at various tip voltages within this range, all pre-

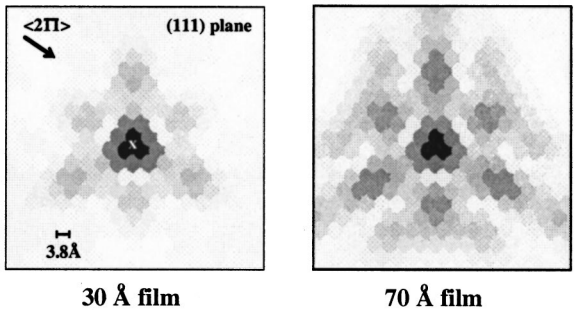

FIG. 3. Left-hand panel: real-space current distribution, $J_{ij}(V=1.5\mathrm{V})$, in a Si_2 layer parallel to the surface after propagation through a 30 Å $CoSi_2(111)$ film. Injection from the tip occurred in the center of the shown plane (white ×), where the maximum current propagating in a focused beam along the ⟨111⟩ direction can still be found. The linear gray scale indicates current intensity at each atomic site: black maximum to white zero current. Right-hand panel: after propagation through a 70-Å film. Note that apart from some increased noise at the sides, the maximum current is still concentrated in a focused beam of approximately the same width as in (a).

sented results will therefore be given for a fixed tip voltage of $E=1.5$ eV, which is well within the validity range of our TB parametrization. The real-space images have been calculated using as much as 1333 special **k** points within the irreducible part of the Brillouin zone, sufficient to suppress any aliasing effects within the computed area of 60 Å ×60 Å centered around the tip position.

Figure 3(a) shows such a current distribution in a bottom Si_2 plane of a $CoSi_2$ trilayer located in 30-Å depth. The current is mainly concentrated on only three atomic sites, directly below the tunneling injection point, despite the distance traveled from the surface. Instead of the spreading predicted by the free-electron model of BEEM, we hence deduce from this figure a strong focalization and a narrowly collimated beam propagating perpendicular through the film. Note that we have chosen a Si_2-type plane, because this is the layer dominantly forming the interface to Si(111).[25] Yet, we stress that the current distribution in any other plane looks very much alike—no significant variation of the beam diameter is noticeable in Si_1 or Co planes. From an intensity-profile cut through the beam along the $\langle 2\bar{1}1\rangle$ direction, a FWHM of 8.9 Å is deduced, cf. Fig. 4, which compares very

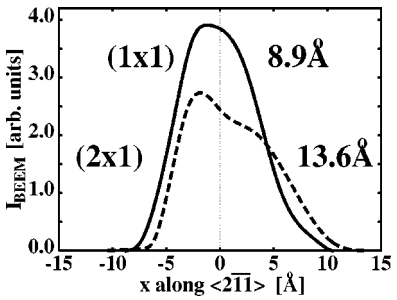

FIG. 4. Intensity profiles through the center of the focused beam along the $\langle 2\bar{1}1\rangle$ direction. An increased FWHM is found in the (2×1) phase (dashed line) compared to the (1×1) (solid line).

well with the above stated experimental value of (11±2) Å, with which the point defects could be resolved. Although we thus achieve a much better agreement compared to the free-electron model, the ≈25-Å beam diameter derived within the latter is not sufficiently off to claim this result as a conclusive confirmation of band-structure effects. Yet, this would be different for thicker films, where the free-electron beam would progressively spread leading to much larger FWHMs. For this reason, we additionally calculated a moderately thick base of 70-Å width. The corresponding current distribution displayed in Fig. 3(b) exhibits a slightly enhanced noise on the sides, but still the form and diameter of the major beam, which carries about one-third of the total current in the plane, have not changed at all. This tells us that the narrow collimation must be an intrinsic feature of ⟨111⟩ oriented $CoSi_2$ films, in which the beam does not have the conical shape shown in Fig. 2(a), but remains instead of constant width as sketched in Fig. 2(b). In this respect it is gratifying that in recent experiments performed with a thicker, 56 Å silicide layer point defects could be resolved with a FWHM of (13±2) Å,[36,37] which is now completely incompatible with the ≈50 Å beam diameter of free-electron theory, but in nice agreement with our calculation.

If the shape of the propagating beam was really dictated by the metal band structure, its focused, constant width would then not be a function of the film thickness, but rather of the area, where electrons are injected initially. To this end, we tested a number of different tip positions, both above highly symmetric and asymmetric sites on the (1×1) Si-rich surface. While the shape of the current distribution obviously reflected the different symmetry, the extracted FWHM of the focused beam was always the same within ±0.1 Å. This suggests an each time almost constant tunneling active area on the surface, representative of the (1×1) Si-rich phase. In addition, the beam was always found to travel exactly perpendicular through the film, hence no beam steering or search-light effect[38] during scans across the surface is expected. This is in accordance with the experimental observation that the position of dislocations and point defects coincided perfectly in the parallel recorded STM and BEEM images.[35]

In the developed picture of a constant beam width, the larger corrugation of the (2×1) phase, should then lead to an enhanced tunneling active area on the surface and in turn to a wider beam as shown in Fig. 2(c). Concomitantly, the calculated current distributions for this phase revealed indeed again a focused beam, yet this time with an increased FWHM of 13.6 Å, cf. Fig. 4, independent of the tip position tested. Note, that also experimentally a decreased resolution had been reported for interface point defects under the (2×1) phase,[39] which nicely corroborates our developed understanding in terms of a focused beam of constant width.

2. Condenser lens effect of the $CoSi_2$ *band structure*

In order to shed more light on the physics behind the fascinating focalization phenomenon, we proceed to analyze the $CoSi_2$ electronic structure. In the relevant energy range 0.9 eV $<E<$2.5 eV, described above, the constant energy surface consists of three nested sheets, the form of which

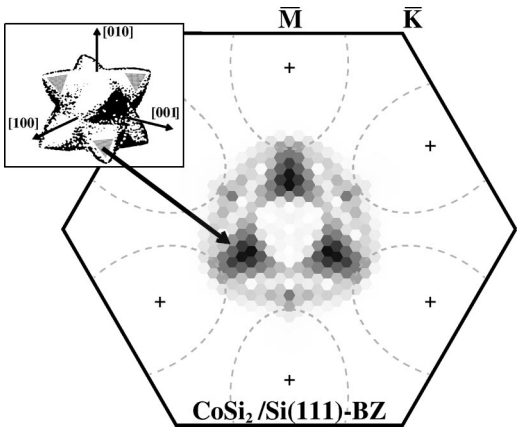

FIG. 5. Reciprocal space-current distribution, $J_{ij}(E=1.5$ eV, $\mathbf{k}_{\|})$, inside the 2D interface Brillouin zone, calculated in the same Si_2 layer as in Fig. 3(a), i.e., after 30-Å film propagation. The current intensity is drawn with a linear gray scale, black representing maximum current. Also drawn are the projections of the Si-conduction-band minima at the chosen energy (dashed lines), defining ellipsoids of available states in the semiconductor. The inset shows the constant energy surface sheet mainly responsible for the current propagation: the shaded black terraces point in the $\langle 111 \rangle$ direction and correspond to the dark areas in the 2D current distribution.

remains practically the same apart from a uniform shrinkage that increases linearly with energy.[30,31] The sheet with the highest group velocity and therefore most influential on transport issues is drawn in the inset of Fig. 5. The star-shaped entity exhibits large flat terraces, which point almost exactly in the $\langle 111 \rangle$ directions. For electrons with appropriate **k** momentum corresponding to a point on these terraces, the silicide band structure acts, therefore, like a condenser lens, keeping the electronic propagation always along a $\langle 111 \rangle$ direction. Following Koster's seminal work,[40] we had shown previously, that especially those regions on the constant energy surface with vanishing curvature are predominantly responsible for the current flow.[9,13] Hence, these leveled terraces represent in addition preferred **k**-space propagation directions.

This reasoning is complemented by the actually calculated current distribution in reciprocal space shown in Fig. 5. The three dark areas, where the majority of the current is concentrated, correspond to the projections of the flat terraces closest to $\bar{\Gamma}$ as depicted by the shaded areas in the inset. All electrons with a $\mathbf{k}_{\|}$ momentum inside these dark patches will travel exactly in the $\langle 111 \rangle$ direction, resulting in a highly focused beam of constant width. Note, however, that the threefold symmetry apparent in Fig. 5 is a mere outcome of the highly symmetric on-top tip position used in this calculation. Notwithstanding, also for less symmetric tip positions the overwhelming fraction of the current is carried on the three flat terraces, see below, whereas it is only the share pertaining to each of the three equivalent ones that differs from case to case. As all these terrace points lead to real space propagation along $\langle 111 \rangle$, a beam with similar FWHM results therefore for all injection points and irrespective of the number of layers traveled.

The focalization of electronic beams passing through $\langle 111 \rangle$ oriented $CoSi_2$ films is thus a material property, induced by the peculiar shape of the current carrying band. As the shape of the latter remains almost constant up to $E=2.5$ eV, a high interface resolution results in the BEEM experiments over quite a voltage range. Interestingly, a recent investigation by Meyer *et al.* showed that the same mechanism is also responsible for the similarly high resolution obtained when injecting hot holes into the metal film.[36] The relevant current carrying band in the valence energy region below E_F has an octahedral shape, again with large-flat terraces pointing in the $\langle 111 \rangle$ directions. The resulting collimated hole beam has an almost constant FWHM of (15 ± 2) Å and (16 ± 2) Å at the interface of a 28-Å - and 56-Å -thick film, respectively.[36] Just like the here described case for electrons, this finding is completely incompatible with the conical shape predicted by classical BEEM theory.[2] It thus appears, as if the focalization feature of the $CoSi_2$ band structure extends over a larger voltage range than discussed in the present study, and might be similarly exploited in future applications involving hot-electron and/or hot-hole propagation.

3. The contrast mechanism

With the reasoning up to this point, we have achieved to explain that an atomically sharp beam would, in principle, allow to resolve pointlike defects at the $CoSi_2$/Si(111) interface. However, this does not yet address the question of the contrast mechanism itself, which makes these objects visible in the experimental BEEM pictures. In order to contribute to the BEEM current, the electrons arriving at the interface have to surmount the Schottky barrier, i.e., in the present case they must have an energy larger than the commonly agreed $eV_0=(0.66\pm0.03)$ eV.[41,42] However, at a perfectly epitaxial interface, the prevailing lateral periodicity would additionally lead to a conservation of $\mathbf{k}_{\|}$ momentum. Hence, the impinging momentum distribution, $J_{ij}(E,\mathbf{k}_{\|})$ shown in Fig. 5, needs to be matched with available semiconductor states. In Si(111) all conduction band minima (CBM) project close to the boundary of the interface Brillouin zone and for the energy range relevant for BEEM no states are present around $\bar{\Gamma}$. The $CoSi_2$ states on the other hand project just in this latter region, so that at the Schottky barrier height eV_0 no state overlapping occurs at all. This situation prevails for about 0.2 eV to higher energies, where the Si CBM widen, but the $CoSi_2$ hole bands narrow. Assuming strict $\mathbf{k}_{\|}$ conservation, no BEEM current should thus be observed up to a delayed onset at about 0.9 eV, where a first overlap between base and collector states occurs.[8]

However, all BEEM experiments performed by von Känel and co-workers gave consistently a Schottky barrier height of $eV_0=(0.66\pm0.05)$ eV.[35–37] Yet, the spectra show additionally a second threshold at ≈0.83 eV,[37] implying that $\mathbf{k}_{\|}$ conservation is apparently violated everywhere at the interface just enough to give the correct Schottky barrier height. Only at the second threshold the $\mathbf{k}_{\|}$ conserving current sets in, finally dominating the total BEEM signal for tip voltages higher than ≈0.9 eV. Notwithstanding, the overlap between

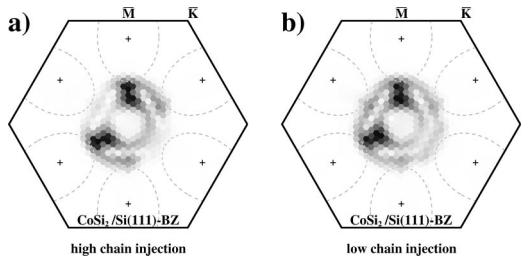

FIG. 6. Reciprocal space-current distribution, $J_{ij}(E=1.5$ eV, $\mathbf{k}_{\|})$, as in Fig. 5, but this time for a (2×1)-terminated surface. (a) Tip position above a high chain, (b) tip position above a low chain.

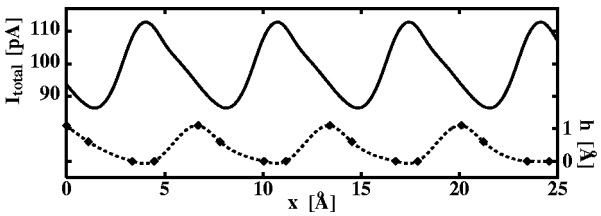

FIG. 7. Total current after 30-Å film propagation (upper curve, left scale) along a simulated scanline perpendicular to the (2×1) chains on the surface, shown in form of a schematic topography (lower curve, right scale). Tip bias is 1.50 eV and the total current has been normalized to 1-nA tunnel injection.

metal and semiconductor states is still small even for such higher biases, cf. Fig. 5. Hence, a decreased amount of $\mathbf{k}_{\|}$ conservation likely to occur each time when the focused beam scans directly over an interfacial point defect, will lead to an enhanced signal, giving rise to the sharp contrast seen in the experimental images.

B. Surface induced contrast in BEEM images

Under (2×1) reconstructed domains, the experimental BEEM images not only showed some scattered point defects, but also exhibited a periodic corrugation reflecting the alternating high- and low-chain structure at the surface.[11] While the high interfacial resolution far beyond the one expected within the classical model only improves the power of the technique in the $CoSi_2/Si(111)$ system, the surface-induced contrast questions the applicability of BEEM as a predominantly interface-sensitive measurement *per se*. In our theoretical analysis of the latter finding, we will first focus on the current propagation within the $CoSi_2$ film. The variation of the magnitude of the total current depending on the tip position found in due course will thereafter be explained in terms of localized surface states, revealing that the latter may significantly influence the measurable BEEM signal.

1. Current propagation under (2×1) *reconstructed surfaces*

Given that the interface to the Si(111), as well as the metal film itself do not depend on the (2×1)-surface structure, but are the same as under (1×1)-terminated domains, the observed surface-induced contrast must have its origin in the initial injection process. Hence, either a change in the energetic or momentum distribution of the tunneling distribution could possibly cause the variations in the BEEM current. Yet, the energetic distribution depends primarily on the mesoscopic vacuum barrier height, which does not exhibit strong changes on an atomic scale. On the other hand, a $\mathbf{k}_{\|}$ redistribution of the injected ensemble depending on the local-sample geometry around the actual tip site would in fact be a reasonable explanation. In Fig. 6, we show the calculated reciprocal space-current distributions, $J_{ij}(E=1.5$ eV, $\mathbf{k}_{\|})$, for a tip position directly above a high chain on the surface (henceforth termed T_1 position), as well as for a tip position above a low chain (henceforth termed T_2). The distributions are almost identical and display the pattern already discussed for the (1×1) phase, i.e., the majority of the current is concentrated in the regions corresponding to the projection of the flat terraces of the constant energy surface sheet. This is what we expected recalling that we also found a narrowly collimated beam under the (2×1)-reconstructed domains, cf. Sec. III A 1.

However, without any significant changes in neither the energetic, nor momentum resolved distribution as a function of the tip position, the only quantity left to show a variation leading to the periodic constrast in the BEEM images, is the total current impinging on the interface itself. To this end, we sum up the detailed current distribution, $J_{ij}(E,\mathbf{k}_{\|})$, inside the complete interface Brillouin zone and integrate over all energies E from the Schottky barrier height to the chosen tip voltage, $eV=1.50$ eV. Interested to see if this quantity exhibits an anticorrugation variation with respect to the film-surface topography, a scanline perpendicular to the $\langle 2\bar{1}1\rangle$ chains is simulated, starting and ending at the tip position T_1 above a high chain up Si atom, while passing midway over the tip position T_2. The minimal height variation during such a tip movement in the experimental constant current mode is neglected, keeping the tip at a fixed 5-Å height and normalizing each time to 1-nA injection by simultaneous computation of the tunnel current. The resulting curve of the total current after 30 Å film propagation is shown in Fig. 7, together with a schematic representation of the surface topography. A striking antiphase modulation with respect to the sequence of alternating high and low chains on the surface is apparent. This is an interesting finding, because we thus find the periodic current variation already inside the metal film itself, completely independent of the interface formed to the Si(111) below, and despite the constant tunneling injection.

In order to figure out the physics behind this anticorrugation, we proceed to narrow down in which part of the silicide film the difference in the magnitude of the total current arises. For this, we follow the current along the different metal layers for the two extreme cases in the scanline, i.e., for the tip positions T_1 and T_2. The curves shown in Fig. 8 display a strong attenuation, which is due to the use of a finite self-energy η in the construction of the Green's functions as described in Sec. II A. Yet, only at long distances this damping yields the expected exponential decay. At short distances, the current presents a much faster decrease, with a $\approx 65\%$ reduction already after the electrons have crossed the top Si bilayer and the first Si_1-Co-Si_2 trilayer. In addition, while the two current curves are exactly the same in these initial 3–4 Å film, the reduction is thereafter slightly larger for electrons being injected above the high chain position.

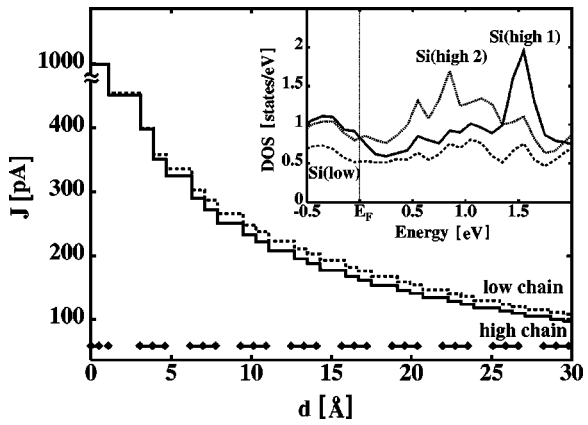

FIG. 8. Total current across the first 30 Å of a $CoSi_2(111)$-(2×1) terminated film: high-chain injection (solid line) vs low-chain injection (dashed line). The diamonds at the bottom indicate the trilayer Si_1-Co-Si_2 sequence in the (111) direction, with the final reconstructed Si chain bilayer. The inset shows the surface density of states projected on the high- and low-chain atoms in the energy region important for BEEM.

This larger loss in comparison to the low chain injection stays almost constant after the crossing of the topmost bulk trilayer and is the direct reflection of the anticorrugation modulation seen in Fig. 7. To check if this finding really leads to the experimentally observed periodic contrast pattern perpendicular to the surface chains, we additionally calculated equivalent current curves for several other tip positions, simulating scan lines either along a high or a low chain. No variation of the total current was found in these cases, so that the theoretical BEEM image of a (2×1) domain would indeed also display a chain-like periodic modulation, irrespective of the interface structure to the Si(111). Note, that no such dependencies of the total current on the tip position, neither a hyperexponential decay in the first 3–4 Å propagation resulted in equivalent computations for (1×1)-terminated films.

2. Role of localized surface states

Knowing that the surface induced contrast in the BEEM images is caused by an unequal current reduction in the topmost 3–4 Å film depending on the tip site, we next focus on the details of the surface electronic structure of the (2×1)-reconstructed domains. The inset in Fig. 8 shows the surface density of states projected onto the different high- and low-chain atoms in the energy range above the Fermi level, which is the one relevant for BEEM applications. Two peaks can be seen, which are each roughly three times more weighted on either of the two high-chain atoms than on the low-chain ones. These peaks can be associated with highly localized-surface bands, predominantly concentrated on the elevated high chains.[26] With the tip positioned directly above this type of chain, obviously a larger fraction of the initial tunnel current will be injected into these states, compared to a tip position above the low chains. This fraction will then not contribute to the current crossing through the metal film, but will rather dissipate laterally away. Keeping in mind that the experiment is performed in the constant current mode, a smaller fraction of the total injected current is then left for the propagating bulk channels, ultimately leading to a diminished current reaching the interface, whenever the tip is located above a high chain.

While this mechanism accounts nicely for a qualitative out of phase modulation of the BEEM current, the absolute magnitude of the effect will strongly depend on the applied bias. The latter controls which share of the total tunnel distribution coincides with the surface state levels. In our case, a 25% variation is found at $eV=1.50$ eV, cf. Fig. 7, and a reduced contrast would result for larger voltages, where most hot electrons possess energies further away from the localized states concentrated in the energy range close to the Fermi level. However, we stress that our argument has been based on the direct elastic current in a semi-infinite film, which is only an approximation to what really impinges on the interface of thin films, subject to multiple reflections and secondary carriers. Nevertheless, although we thus do not expect a perfect agreement with the experimental data, we are still reasonably close to the $\approx 7\%$ corrugation measured at $eV=2.00$ eV.[11]

It is finally worth mentioning, that the suggested mechanism may certainly apply for other systems as well, although such a clearcut influence of the surface electronic structure has hitherto been completely neglected in the BEEM data analysis. Localized surface states[43,44] may just as much exist below the Fermi level, so that also reverse-bias BEEM or hole BEEM on *p*-type semiconductor substrates[2] may be affected. Especially the experimentally observed, atomic-scale variations of the BEEM current on two different terminations of $CoSi_2$/Si(100) samples under forward and reverse voltages[11] seem likely candidates for this effect in view of the numerous dangling bonds present in these structures.[32] Further, more general consequences are also conceivable along this line of thought: The often reported clear correlation between surface topographic protrusions, like steps, and pronounced local changes in the microscopic BEEM images has, e.g., usually been attributed to beam steering due to a tilted injection cone,[2] i.e., a beam shape as shown in Fig. 2(a), but tilted to one side because of the surface propension at a step. Since this (mesoscopic) free-electron picture is not very compatible with the idea of preferred propagation directions dictated by the metallic band structure, it is tempting to reassess these findings in terms of small-scale influences of the surface electronic structure, which as we have just shown, may also lead to distinct contrast in the recorded BEEM images. Although this generic assertion needs logically to be scrutinized with detailed calculations for each individual system, already the particular results for the $CoSi_2$/Si(111) surfaces discussed in this work raise a suspicion of how delicate the interface geometric information in BEEM images may be meshed with details of the electronic properties of the metallic overlayer, and of how elaborate a theory is required to carefully interpret such data.

IV. SUMMARY

In the present work we have applied our theoretical model of BEEM, which in contrast to the prevalent Bell-Kaiser

model[1,2] takes the metallic band structure fully into account, to analyze experimental BEEM data for the $CoSi_2/Si(111)$ system. In order to properly analyze the experimental measurements done on ultrathin, extremely well-defined films, we have extended our previous model to correctly include the detailed surface geometric and electronic structure. The two most salient and hitherto unexplicable experimental findings were an unprecedented quasi-atomic resolution of interface point defects[34,36] and a surface-induced contrast in the BEEM images, reflecting the alternating high- and low-chain topography of a (2×1)-reconstructed surface.[11] Both effects could be traced back to peculiarities of the $CoSi_2$ band structure. The latter acts like a condenser lens on electrons propagating in the $\langle 111\rangle$ direction through the metallic film, leading to a narrowly collimated beam, whose width is independent of the number of layers crossed and that is small enough to achieve the atomic resolution. While this finding nicely enhances the power of BEEM as an *interface*-sensitive technique, we could show on the other hand, that localized *surface* states on the high-chain atoms in the (2×1) domains are responsible for the reported periodic contrast. When the tip is located on top of such high-chain atoms, a larger fraction of the current is injected into these surface bands, leaving a diminished current to arrive at the interface and thus resulting in a periodic anticorrugation modulation in the BEEM signal.

Although the focus of the present work has been the detailed analysis of particular experimental data for the $CoSi_2/Si(111)$ system, the disclosed strong dependence on the electronic structure of the metal overlayer raises a conclusion, which addresses BEEM in general. Originally the technique had been developed on rather ill-defined systems, like Au/Si contacts involving relatively thick films. The classical Bell-Kaiser model of BEEM developed alongside with these early measurements was intended and sufficient for a *qualitative* understanding of such data. The later methodological refinement and the application of BEEM to coherent and quasiperfect systems like the $CoSi_2/Si(111)$ contacts invariably requires a much more involved theoretical modeling, which among other factors needs to fully take into account the metal-band structure. BEEM certainly is highly sensitive to interfacial properties, but the resulting data is intricately influenced by the electronic properties of the metal overlayer, requiring a careful and elaborate theory in order to carefully interpret the experimental measurements.

ACKNOWLEDGMENTS

We would like to thank Thomas Meyer and Hans von Känel for their readiness to explain subtle experimental details to theorists. K.R. and K.H. are grateful for financial support from SFB 292 (Germany). Financial support from the Spanish CICYT under Contracts Nos. PB98-524 and PB97-28 is acknowledged.

*Present address: Fritz-Haber Institut der Max-Planck Gesellschaft, Faradayweg 4-6, 14195 Berlin (Germany).

[1] W. J. Kaiser and L. D. Bell, Phys. Rev. Lett. **60**, 1406 (1988); **61**, 2368 (1988).
[2] M. Prietsch, Phys. Rep. **253**, 163 (1995).
[3] P.L. de Andres, F.J. Garcia-Vidal, K. Reuter, and F. Flores, Prog. Surf. Sci. **66**, 1 (2001).
[4] A.M. Milliken, S. J. Manion, W. J. Kaiser, L. D. Bell, and H. Hecht, Phys. Rev. B **46**, 12 826 (1992).
[5] L.J. Schowalter and E.Y. Lee, Phys. Rev. B **43**, 9308 (1991).
[6] R. Ludeke, Phys. Rev. Lett. **70**, 214 (1993).
[7] U. Hohenester, P. Kocevar, P.L. de Andres, and F. Flores, phys. stat. sol. **204**, 397 (1997); cond-mat/9710151 (unpublished).
[8] M.D. Stiles and D.R. Hamann, J. Vac. Sci. Technol. B **9**, 2394 (1991).
[9] F.J. Garcia-Vidal, P.L. de Andres, and F. Flores, Phys. Rev. Lett. **76**, 807 (1996).
[10] H. von Känel, Mater. Sci. Rep. **8**, 193 (1992).
[11] H. Sirringhaus, E.Y. Lee, and H. von Känel, Phys. Rev. Lett. **74**, 3999 (1995); Surf. Sci. **331**, 1277 (1995).
[12] C. Caroli, R. Combescot, P. Nozieres, and D. Saint-James, J. Phys. C **5**, 21 (1972).
[13] K. Reuter, P.L. de Andres, F.J. Garcia-Vidal, D. Sestovic, F. Flores, and K. Heinz, Phys. Rev. B **58**, 14 036 (1998).
[14] F. Guinea, C. Tejedor, F. Flores, and E. Louis, Phys. Rev. B **28**, 4397 (1983).
[15] M. Lannoo and P. Friedel, *Atomic and Electronic Structure of Surfaces* (Springer-Verlag, Berlin, 1991).
[16] P.L. de Andres, F.J. Garcia-Vidal, D. Sestovic, and F. Flores, Phys. Scr., T **T66**, 277 (1996).
[17] K. Reuter, P.L. de Andres, F.J. Garcia-Vidal, D. Sestovic, F. Flores, and K. Heinz, Comput. Phys. Commun. **127**, 327 (2000).
[18] E.Y. Lee, H. Sirringhaus, U. Kafader, and H. von Känel, Phys. Rev. B **52**, 1816 (1995).
[19] K. Reuter, P.L. de Andres, F.J. Garcia-Vidal, F. Flores, U. Hohenester, and P. Kocevar, Europhys. Lett. **45**, 181 (1999).
[20] K. Reuter, U. Hohenester, P.L. de Andres, F.J. Garcia-Vidal, F. Flores, and K. Heinz, Phys. Rev. B **61**, 4522 (2000).
[21] R.W.G. Wyckoff, *Crystal Structures*, 2nd ed. (Interscience, New York, 1963).
[22] S.A. Chambers, S.B. Anderson, H.W. Chen, and J.H. Weaver, Phys. Rev. B **34**, 913 (1986).
[23] F. Hellman and R.T. Tung, Phys. Rev. B **37**, 10 786 (1988).
[24] R. Stalder, H. Sirringhaus, N. Onda, and H. von Känel, Surf. Sci. **258**, 153 (1991).
[25] A. Seubert, J. Schardt, W. Weiss, U. Starke, K. Heinz, and Th. Fauster, Appl. Phys. Lett. **76**, 727 (2000).
[26] K. Reuter, P.L. de Andres, F.J. Garcia-Vidal, F. Flores, and K. Heinz, Appl. Surf. Sci. **166**, 103 (2000).
[27] L. Haderbache, P. Wetzel, C. Pirri, J.C. Perruchetti, D. Bolmont, and G. Gewinner, Phys. Rev. B **39**, 12 704 (1989).
[28] J.C. Slater and G.F. Koster, Phys. Rev. **94**, 1498 (1954).
[29] S. Sanguinetti, C. Calegari, V.R. Velasco, G. Benedek, F. Tavazza, and L. Miglio, Phys. Rev. B **54**, 9196 (1996).
[30] W.R.L. Lambrecht, N.E. Christensen, and P. Blöchl, Phys. Rev. B **36**, 2493 (1987).
[31] L.F. Mattheiss and D.R. Hamann, Phys. Rev. B **37**, 10 623 (1988).
[32] R. Stadler, R. Podloucky, G. Kresse, and J. Hafner, Phys. Rev. B

57, 4088 (1998); R. Stadler, Ph.D. thesis, Technische Universität Wien, 1997.
[33] C. Pirri, G. Gewinner, J.C. Peruchetti, D. Bolmont, and J. Derrien, Phys. Rev. B **38**, 1512 (1988); C. Pirri, P. Wetzel, J.C. Peruchetti, D. Bolmont, G. Gewinner, K. Hricovini, and J. Bonnet, Appl. Surf. Sci. **56**, 507 (1992).
[34] T. Meyer and H. von Känel, Phys. Rev. Lett. **78**, 3133 (1997).
[35] H. Sirringhaus, E.Y. Lee, and H. von Känel, Phys. Rev. Lett. **73**, 577 (1994); J. Vac. Sci. Technol. B **12**, 2629 (1994).
[36] T. Meyer, D. Migas, L. Miglio, and H. von Känel, Phys. Rev. Lett. **85**, 1520 (2000).
[37] H. von Känel and T. Meyer, J. Cryst. Growth **210**, 401 (2000).
[38] M. Prietsch and R. Ludeke, Phys. Rev. Lett. **66**, 2511 (1991); Surf. Sci. **251**, 413 (1991).
[39] H. Sirringhaus, T. Meyer, E.Y. Lee, and H. von Känel, Surf. Sci. **357**, 386 (1996); Phys. Scr., T **T66**, 282 (1996).
[40] G.F. Koster, Phys. Rev. **95**, 1436 (1954).
[41] J.Y. Duboz, P.A. Badoz, F. Arnaud d'Avitaya, and E. Rosencher, Phys. Rev. B **40**, 10 607 (1989).
[42] H. von Känel, J. Henz, M. Ospelt, J. Hugi, E. Müller, and N. Onda, Thin Solid Films **184**, 295 (1990).
[43] K. Reuter, F.J. Garcia-Vidal, P.L. de Andres, F. Flores, and K. Heinz, Phys. Rev. Lett. **81**, 4963 (1998).
[44] M.K. Weilmeier, W.H. Rippard, and R.A. Buhrman, Phys. Rev. B **59**, R2521 (1999).